

Gold Nanoparticles with Self-Assembled Cysteine Monolayer Coupled to Nitrate Reductase in Polypyrrole Matrix Enhanced Nitrate Biosensor

Thangamuthu Madasamy¹, Manickam Pandiaraj¹, Anantha Koteswararao Kanugula³, Seenivasan Rajesh¹, Kalpana Bhargava², Niroj Kumar Sethy², Sririgidhar Kotamraju³, and Chandran Karunakaran^{1,*}

¹Biomedical Research Laboratory, Department of Chemistry, VHNSN College, Virudhunagar 626001, Tamil Nadu, India

²Peptide and Proteomics Division, DIPAS, DRDO, Delhi 110054, India

³Center for Chemical Biology, CSIR-Indian Institute of Chemical Technology, Hyderabad 500607, India

We have developed here a novel, highly sensitive and selective nitrate (NO_3^-) biosensor by covalent immobilization of nitrate reductase (NaR) in self-assembled monolayer (SAM) of cysteine on gold nanoparticles (GNP)-polypyrrole (PPy) modified platinum electrode. Incorporation of GNP in highly microporous PPy matrix was confirmed by morphological scanning electron microscope (SEM) images. The electrochemical behavior of the NaR modified electrode exhibited the characteristic reversible redox peaks at the potential, -0.76 and -0.62 V versus Ag/AgCl. Further, the GNP-PPy nanocomposite enhanced the current response by 2-fold perhaps by enhancing the immobilization of NaR and also direct electron transfer between the deeply buried active site and the electrode surface. The common biological interferences like ascorbic acid, uric acid were not interfering with the NO_3^- measurement at low concentration levels. This biosensor showed a wide linear range of response over the concentration of NO_3^- from $1 \mu\text{M}$ to 1mM , with higher sensitivity of $84.5 \text{ nA } \mu\text{M}^{-1}$ and a detection limit of $0.5 \mu\text{M}$. Moreover, the NO_3^- level present in the nitrate-rich beetroot juice and the NO_3^- release from the lipopolysaccharide treated human breast cancer cells were estimated.

KEYWORDS: Beetroot Juice, Cancer Cells, Gold Nanoparticles, Nitrate Reductase, Nitrate Biosensor, Direct Electron Transfer.

1. INTRODUCTION

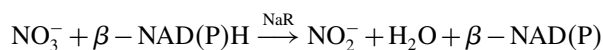
Inorganic nitrate (NO_3^-) anion is generally believed to be an inert oxidative product of nitric oxide (NO) metabolism and potentially toxic for food chain.¹ However, recent research reports suggest existence of an alternate Nitrate–Nitrite–NO pathway promoting NO bioavailability and signaling during ischemia and hypoxia.² Administration of exogenous NO_3^- to human and several animal models reportedly promotes NO-like bioactivity and regulates biological activities like reduction of blood pressure, vasodilation, cytoprotection, cardioprotection, protection from ischemia-reperfusion injury as well as promotes exercise capacity.^{3–5} Interestingly, the vegetables like beetroot, spinach, and lettuce along with cured meat in our everyday diet is a major source of inorganic nitrate.⁶ Recent

perspective observational investigations have also shown that higher intake of nitrate-rich fruits and vegetables are associated with reduced risk of coronary and ischemic heart diseases.^{7,8} Hence, the measurement of NO_3^- level present in the beetroot juice give a supporting information to prove the natural remedy effect of beetroot juice against cardiovascular diseases and blood pressure. Moreover, the measurement of NO_3^- release during lipopolysaccharide (LPS) induced apoptosis in cancer cells and macrophages give an idea to know the molecular mechanisms by which LPS exert cytotoxicity.⁹ So, the determination of NO_3^- is increasingly important in biology and medicine.

In the literature, various methods have been reported for the determination of NO_3^- including spectrophotometry,^{10,11} fluorescence,^{12,13} ion-exchange chromatography.¹⁴ These methods were time consuming and not sufficiently specific. Recently, electrochemical biosensor techniques are proved to be powerful tools due to their advantages of simplicity, portability, inexpensive and fast analysis in combination with high selectivity.^{15–20}

*Author to whom correspondence should be addressed.
Email: ckaru2000@gmail.com
Received: 22 June 2012
Accepted: 6 August 2012

The enzymatic^{21, 22} and non-enzymatic^{23, 24} electrochemical methods have been reported for the determination of NO_3^- . Among these, the enzymatic method has been widely performed using nitrate reductase (NaR). NaR is a multidomain enzyme containing flavin adenine dinucleotide (FAD), two heme-Fe and molybdopterin, which catalyzes the two electron reduction of NO_3^- to NO_2^- .²⁵



The stable immobilization of an enzyme on an electrode surface with complete retention of its biological activity is a crucial problem for the commercial development of biosensors. During the last decades, conducting polymers have attracted much interest as a suitable matrix for the entrapment of enzymes.²⁶ Among the conducting polymers, polypyrrole (PPy) was widely used owing to its high electrical conductivity, good stability and easy to fabricate on the electrode surface.²⁷ Further, modification of electrode surface with gold nanoparticles (GNP) provides a microenvironment similar to that of the redox proteins in the native systems due to its large surface-to-volume ratio, increased surface activity and electronic properties.²⁸ Also, thiols on GNP forms highly ordered and stable self-assembled monolayer (SAM). These well ordered monolayers offer the possibility to covalently fix proteins close to an electrode surface, further the electrical wiring of PPy/GNP nanocomposite functioning as electron conducting pathways between the deeply buried prosthetic groups and the electrode.

Hence, in this work, we have covalently coupled the NaR, a multidomain enzyme to the SAM of cysteine on GNP in PPy matrix. This NaR modified electrode exhibited the higher sensitivity because of the facilitated electron transfer and enhanced loading of NaR at the SAM-GNP-PPy-Pt electrode. For the first time, we have estimated here the NO_3^- level present in the beetroot juice using this biosensor and validated with the griess method. Further, the NO_3^- release from LPS treated human breast cancer cells was also estimated.

2. EXPERIMENTAL DETAILS

2.1. Reagents

Nitrate reductase from *Aspergillus niger*, chloroauric acid trihydrate ($\text{HAuCl}_4 \cdot 3\text{H}_2\text{O}$), β -NADPH, sulphanilic acid, *N*-(1-naphthyl)ethylenediamine dihydrochloride, cysteine, sodium ascorbate, uric acid, sodium hydrogen phosphate, disodium hydrogen phosphate, pyrrole, NaNO_3 , KCl and LPS were obtained from Sigma Company (Milwaukee, WI, USA). Nitrate supplement beetroot juice was obtained from Defence Food Research Laboratory, Mysore, India. MCF-7 breast cancer cells were obtained from ATCC. All the solutions were prepared with doubly distilled water.

2.2. MCF-7 Cell Culture

MCF-7 cells were grown in 10% minimum essential medium (MEM) containing 10% fetal bovine serum (FBS), l-glutamine (4 mmol L^{-1}), penicillin ($100 \text{ units mL}^{-1}$) and streptomycin ($100 \mu\text{g mL}^{-1}$), and incubated at 37°C in a humidified atmosphere of 5% CO_2 and 95% air.

2.3. Instrumentations

All the electrochemical experiments were performed using CHI 1200B electrochemical workstation (CHI, USA) with a conventional three electrode system which consisted of an Ag/AgCl wire as reference electrode, a Pt wire as auxiliary or counter electrode and a Pt electrode with NaR immobilized in SAM-GNP-PPy as the working electrode. The size of Pt wire working electrode was 0.5 mm in diameter. Spectrophotometric studies were carried out using shimadzu 1800 UV spectrophotometer (Shimadzu scientific instruments Inc.). The SEM morphological images of GNP-PPy-Pt, PPy-Pt and bare Pt electrodes were obtained using a FEI Quanta FEG 200-High Resolution Scanning Electron Microscope (FEI Co., Netherlands).

2.4. Synthesis of Gold Nanoparticles (GNP)

GNP was prepared as per earlier report²⁹ by adding 40 ml of 0.1 M solution of $\text{HAuCl}_4 \cdot 3\text{H}_2\text{O}$ and 60 ml of 0.1 M D-glucose to about 2 ml of 0.2% soluble starch followed by 15 ml of 1 M NaOH. The solution remained colorless for the initial 30 min, following which it turned red slowly, indicating the formation of GNP. The GNP was stable for several months, as confirmed by its surface plasmon resonance peak at around 525 nm.

2.5. Construction of NaR-SAM-GNP-PPy-Pt Electrode

2.5.1. Pyrrole Electropolymerization

Prior to electropolymerization, the electrode was polished with alumina powder (size 0.05 and $1.0 \mu\text{m}$) until to get a highly shining surface and washed twice with double distilled water. Finally, the electrode was cleaned in 1 M H_2SO_4 by cycling the potential from -200 to $+1450 \text{ mV}$ versus Ag/AgCl until to attain reproducible cyclic voltammograms (CVs) and then washed with double distilled water. PPy films were electropolymerized and electroadsorbed³⁰ on to the bare Pt electrode from a deaerated solution of 0.4 M pyrrole using 0.1 M KCl as supporting electrolyte, at the potential between 0.0 and $+0.9 \text{ V}$ versus Ag/AgCl with a scan rate of 50 mV s^{-1} , for 10 complete cycles.³¹ The pyrrole polymerization was carried out under argon atmosphere at room temperature.

2.5.2. Formation of the SAM-GNP-PPy Nanocomposite and Immobilization of NaR

The obtained PPy-Pt electrode was immersed in GNP solution for 10 h and then carefully rinsed with double distilled water. GNP was incorporated into the microporous PPy matrix perhaps via the electrostatic attraction.³² Further, the GNP-PPy-Pt electrode modified with the SAM of cysteine was prepared by dipping the previously GNP incorporated PPy-Pt electrode into a 1 mM cysteine solution for 20 min and rinsed with double distilled water to remove the non-chemisorbed cysteine. Then, 5 μL of NaR (0.2 g mL^{-1}) enzyme solution was dropped onto SAM-GNP-PPy-Pt modified electrode. After that, the electrode was left for 24 h at 4 $^{\circ}\text{C}$. During this process, the NaR is covalently coupled on SAM-GNP-PPy-Pt electrode. The preparation of this modified electrode is shown in Scheme 1. This NaR modified electrode was immersed in 0.1 M PBS to remove the loosely adsorbed NaR and was stored at 4 $^{\circ}\text{C}$ when not in use.

3. RESULTS AND DISCUSSION

The majority of sensor devices utilize many conducting polymers (polyaniline, polypyrrole and polyacetylene) with definite roles, either in the sensing mechanism or through immobilizing the species responsible for sensing of the analyte component. In this study, we have incorporated GNP in the highly porous PPy matrix on the electrode surface. Further, SAM of cysteine on GNP in PPy matrix enhanced the immobilization of NaR to achieve high sensitivity for the determination of NO_3^- . In order to test the performance of the developed NO_3^- biosensor, sensitivity, life time, scan rate, pH and selectivity were investigated.

3.1. Characterization of GNP by UV-Visible Spectroscopy

The typical UV-visible absorption spectrum of the synthesized GNP exhibited λ_{max} at 525 nm. The peak intensity

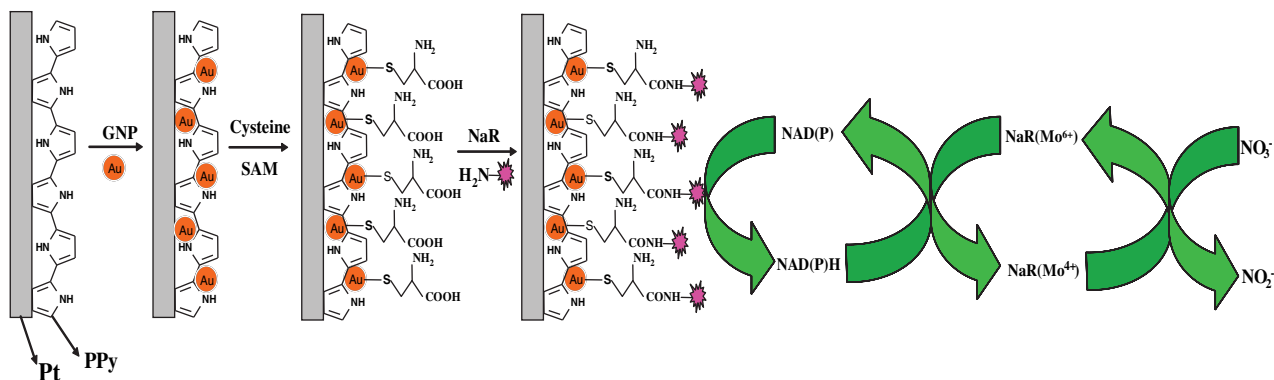
and position of the surface plasmon absorption band was earlier reported to be dependent on the size and geometry of the metal nanoparticles as well as the medium surrounding the particles. It was reported that the spherical particles with diameters around 6–10 nanometers characterized by HR-TEM showed a strong absorption peak in the visible region of the UV-visible spectrum.²⁹ Thus, the observed peak at 525 nm here clearly revealed the formation of GNP.

3.2. Morphological Characterization of Electrodes Using SEM

Figures 1(a)–(c) show the SEM morphological images of bare Pt, PPy-Pt and GNP-PPy-Pt electrodes respectively. Figure 1(b) reveals the typical highly porous morphology of PPy on Pt electrode surface. This high porous nature of PPy perhaps provides much larger surface area to incorporate more GNP and hence NaR at the electrode surface. Further, the SEM of GNP-PPy-Pt (Fig. 1(c)) electrode shows the gold nanoparticles were distributed on the PPy matrix.

3.3. Electrochemical Characterization of the Modified Electrodes

Figure 2 shows the typical CV obtained for the bare Pt (curve a), PPy-Pt (curve b), GNP-PPy-Pt (curve c), NaR-PPy-Pt (curve d) and NaR-SAM-GNP-PPy-Pt (curve e) electrodes at a scan rate of 50 mV s^{-1} in 0.1 M PBS at pH 7.0. The broad peaks were observed on the CV range of -0.9 V to -0.3 V for the PPy-Pt and GNP-PPy-Pt electrodes perhaps due to the complex redox process of PPy³³ and also high capacitive currents.³⁴ However, the CV of NaR immobilized on both the PPy-Pt and SAM-GNP-PPy-Pt electrodes exhibited well-defined reversible redox peaks at -0.76 and -0.62 V versus Ag/AgCl with decreased capacitive currents. When enzyme was adsorbed on the electrode surface, the capacitive currents in the double-layer regions decreased because the proteinaceous layer



Scheme 1. Schematic representation of the preparation of NaR-SAM-GNP-PPy-Pt electrode and the illustration of the reactions during the determination of NO_3^- .

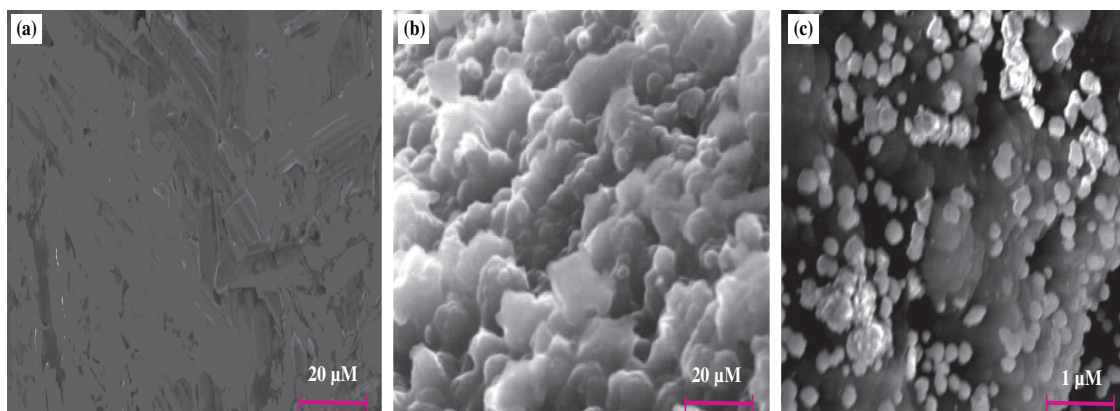


Fig. 1. SEM micrographs of (a) bare Pt, (b) PPy-Pt and (c) GNP-PPy-Pt electrodes.

was formed. This interaction with the electrical double layer (Helmholtz double layer) at the electrode severely hindered the electron transfer rates between the electrode surface and the electrolyte.³⁴ Consequently, the Helmholtz distance (between the Helmholtz layer and the electrode) increased; hence the electrical double layer may be forced away from the electrode surface.³⁵ So, the capacitive currents obtained for the NaR modified electrode decreased (curve d and curve e) when compared to without NaR (curve b and curve c). The observed reversible redox peaks are further attributed to the Mo(IV/VI) complex moiety of NaR in agreement with the previously reported data.²⁵ It clearly reveals that the NaR was immobilized on the electrode surface.

It is further evident from the Figure 2 that the NaR-SAM-GNP-PPy-Pt electrode (curve e) shows increase in current than the NaR-PPy-Pt electrode (curve d). This is perhaps due to the large number of NaR molecules firmly coupled on the SAM of cysteine on GNP in PPy matrix and also the facilitated electron transfer between

the electrode and the active site of the NaR. The well-defined reversible redox peaks obtained due to NaR and the current observed were stable; for instance, it remained essentially unchanged when the potential scan was continuously repeated at 50 mV s^{-1} for 10 min.

3.4. Electrochemical Response to NO_3^-

Figure 3 shows the electrochemical response of the bare Pt, NaR-PPy-Pt and NaR-SAM-GNP-PPy-Pt electrodes in the absence (a, b and d) and presence (c and e) of $500 \mu\text{M}$ NO_3^- in 0.1 M PBS (pH 7.0) measured at the scan rate of 50 mV s^{-1} versus Ag/AgCl. After the addition of NO_3^- , the current response at the bare Pt electrode is same as without NO_3^- (data not shown). However, the current is significantly increased in both the NaR-PPy-Pt (curve c) and NaR-SAM-GNP-PPy-Pt (curve e) electrodes cathodically as well as anodically. It is due to the enhanced electrocatalytic activity of the NaR-modified electrodes based

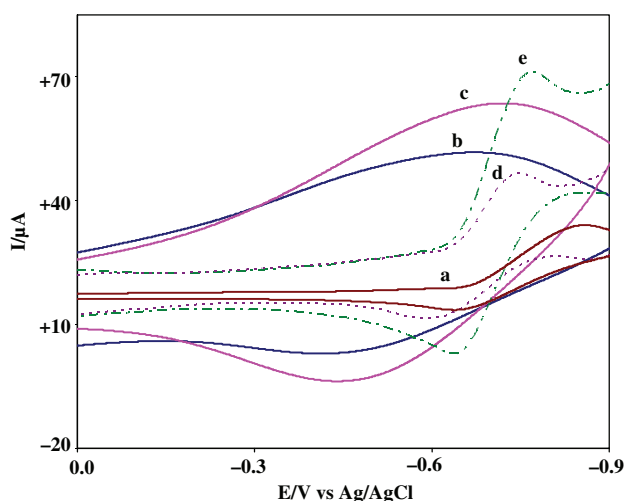


Fig. 2. Typical CV response of (a) bare Pt, (b) PPy-Pt, (c) GNP-PPy-Pt, (d) NaR-PPy-Pt and (e) NaR-SAM-GNP-PPy-Pt electrodes in 0.1 M PBS (pH 7.0) at scan rate: 50 mV s^{-1} versus Ag/AgCl.

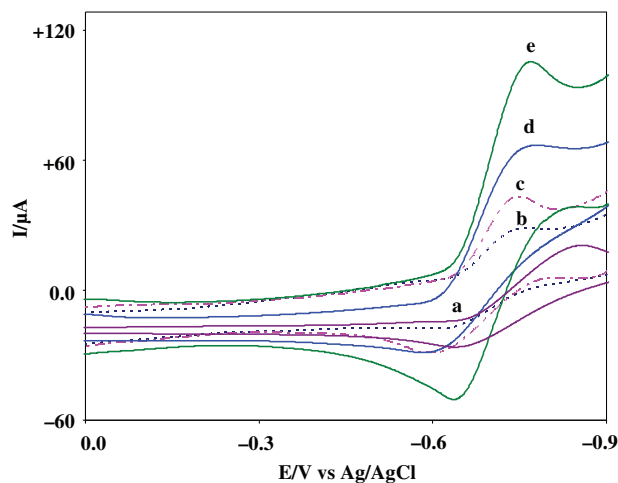


Fig. 3. Electrochemical response of bare Pt, NaR-PPy-Pt and NaR-SAM-GNP-PPy-Pt electrodes in the absence (a, b and d) and presence (c and e) of $500 \mu\text{M}$ NO_3^- in 0.1 M PBS at scan rate: 50 mV s^{-1} versus Ag/AgCl.

on the intrinsic specificity of the NaR which catalyzes the reduction of NO_3^- to NO_2^- via a cyclic redox reaction of its Mo(IV/VI) complex moiety (Scheme 1).

3.5. Effect of Gold Nanoparticles

Figure 4 compares the CV's of NaR-SAM-GNP-PPy-Pt and NaR-PPy-Pt electrodes in 0.1 M PBS containing 200 μM NO_3^- . It is obviously seen that the current response of the NaR-SAM-GNP-PPy-Pt electrode is 2-fold (40 μA) greater than that of the NaR-PPy-Pt electrode at -0.76 V. This observed increase in current suggest that the SAM of cysteine on GNP perhaps provided more surface area to couple NaR effectively and also a desirable orientation, environment to facilitate the direct electron transfer between the active site of the NaR and the base electrode.

3.6. Effect of pH and Scan Rate

The electrochemical behavior of the NO_3^- biosensor was studied in the pH range of 3.0–10.0. For the pH study, a mixture of disodium hydrogen phosphate and citric acid buffer was used. The current response was decreased from pH 7.0–3.0 and also from pH 7.0–10.0, perhaps due to the denaturation of immobilized NaR. However, the maximum current response was observed at pH 7.0 (Fig. 5(A)).

Further, the influence of the scan rate on the CV performance of the NaR-SAM-GNP-PPy-Pt electrode was investigated (Fig. 5(B)). It was found that the cathodic peak currents increased linearly with increasing the scan rate from 50 to 250 mV s^{-1} and also the characteristic CV remains unchanged on successive potential scanning upto 250 mV s^{-1} . This indicates the favorable orientation of NaR at the SAM-GNP-PPy-Pt electrode leading to a facilitated electron transfer of NaR.

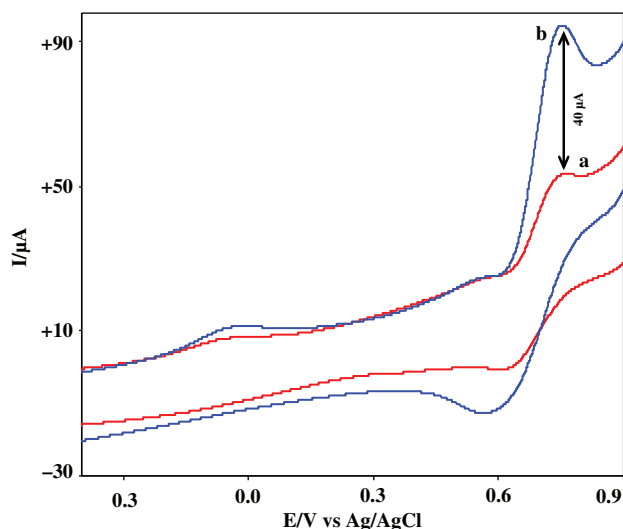


Fig. 4. Typical CV response of (a) NaR-PPy-Pt and (b) NaR-SAM-GNP-PPy-Pt electrodes in 0.1 M PBS containing 200 μM NO_3^- at scan rate: 50 mV s^{-1} versus Ag/AgCl.

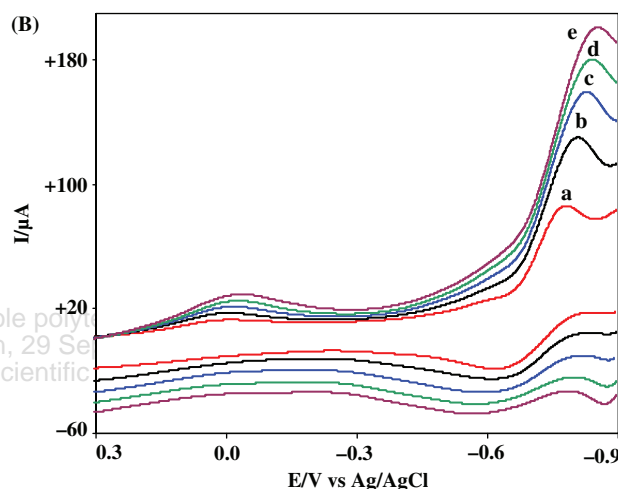
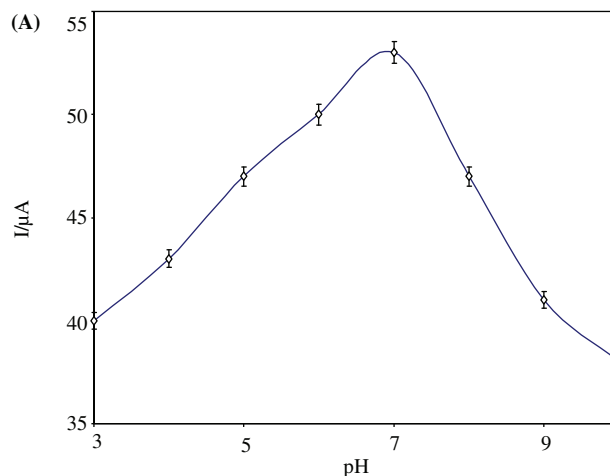


Fig. 5. (A) Effect of pH on peak current of NaR-SAM-GNP-PPy-Pt electrode in 0.1 M PBS at scan rate: 50 mV s^{-1} versus Ag/AgCl. Each point represents the average of three measurements. (B) Effect of increasing scan rate from 50 to 250 mV s^{-1} on NaR-SAM-GNP-PPy-Pt electrode in 0.1 M PBS containing 200 μM of NO_3^- solution.

3.7. Linearity, Selectivity, Stability and Reproducibility

Typical CVs were obtained for several concentrations of NO_3^- in 0.1 M PBS at 50 mV s^{-1} for NaR-SAM-GNP-PPy-Pt and are shown in Figure 6(A). The observed cathodic currents versus NO_3^- concentrations are plotted as shown in Figure 6(B). The calibration curve thus obtained for NaR-SAM-GNP-PPy-Pt electrode exhibits a linear range of response for the NO_3^- concentrations from 1 μM to 1 mM ($r^2 = 0.9837$, $n = 3$) with a detection limit of 0.5 μM .

Moreover, the NaR-SAM-GNP-PPy-Pt electrode shows the excellent electroanalytical performance; for instance, wider linear detection range and especially high sensitivity, compared to the other reported NO_3^- biosensors (Table I).

It is well-known that coexisting biological substrates viz ascorbic acid (AsA) and uric acid (UA) present at high

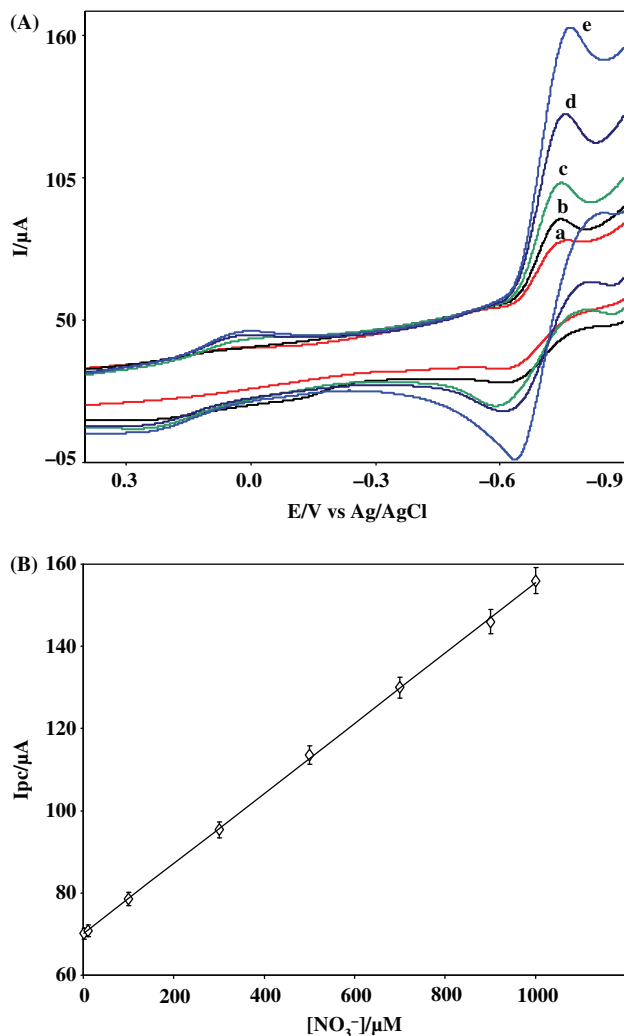


Fig. 6. (A) Typical CV response of NaR-SAM-GNP-PPy-Pt electrode (a) 100 μM , (b) 200 μM , (c) 400 μM , (d) 700 μM and (e) 1000 μM of NO_3^- in 0.1 M PBS (pH 7.0) at scan rate: 50 mV s^{-1} versus Ag/AgCl. (B) A linear calibration plot for the cathodic peak currents I_{pc} versus $[\text{NO}_3^-]/\mu\text{M}$. ($I_{pc} = 0.0624[\text{NO}_3^-] + 52.332$, $r^2 = 0.9837$). Each point represents the average of three measurements.

levels may interfere in the electrochemical determination of NO_3^- . When these interferences were added into the 0.1 M PBS containing 500 μM NO_3^- (Fig. 7), there were only slight changes observed. Also, the time versus current response of the biosensor for the addition of 500 μM

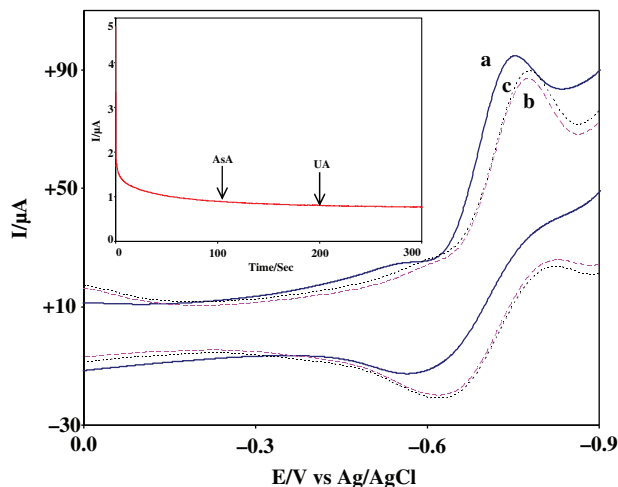


Fig. 7. Typical CV response of NaR-SAM-GNP-PPy-Pt electrode (a) 500 μM NO_3^- , (b) 500 μM NO_3^- + 500 μM UA and (c) 500 μM NO_3^- + 500 μM AsA in 0.1 M PBS (pH 7.0) at scan rate: 50 mV s^{-1} versus Ag/AgCl. The chronoamperometric response of the NaR-SAM-GNP-PPy-Pt electrode in 0.1 M PBS containing 500 μM NO_3^- in the presence of 500 μM of AsA and UA (Inset of Fig. 7).

each of AsA and UA was studied chronoamperometrically (shown as inset in Fig. 7) and obtained no changes in the currents. For the stability and reproducibility test, cathodic responses for NO_3^- were recorded three times daily and the current responses were found to be constant for one month, which holds relatively longer stability than other NO_3^- biosensors.

3.8. Determination of NO_3^- Levels in Beetroot Supplement

Beetroot juice, which contains a high level of nitrate, substantially decreases blood pressure (BP) levels, inhibits platelet aggregation and prevents ischemia-induced endothelial dysfunction [www.sciencedaily.com]. In this study, we attempted to measure the NO_3^- level present in the beetroot supplement using our highly sensitive NO_3^- biosensor. The cathodic peak current of the NaR-SAM-GNP-PPy-Pt electrode obtained for the beetroot juice was compared with the linear calibration curve (Fig. 6(B)) reveals that the concentration of NO_3^- is present in the range of $600 \pm 12 \mu\text{M}$. Further, this result was validated with the standard griess method and found that $602 \pm 12.0 \mu\text{M}$ of NO_3^- is present. In order to make sure these results, the same measurement was carried out thrice

Table I. The electroanalytical properties of the NO_3^- biosensor.

Electrodes	Linearity	Sensitivity	Detection limit	Ref.
NaR/MV ²⁺ -PPy/GCE	35 μM –3 mM	13.8 mA/M	0.4 μM	24
NaR/Ni ^b /MV ²⁺ /Au ^c	20 μM –250 μM	—	5 μM	36
PS ^d /NaR/GCE ^e	5 μM –0.4 mM	60 mA/M	4.5 μM	37
NaR/PPy/Pt	100 μM –5 mM	—	15 μM	38
NaR/SAM/GNP/PPy/Pt	1 μM –1 mM	84.5 mA/M	0.5 μM	Present work

^aMethyl viologen, ^bNafion, ^cGold, ^dPhenosafranin, ^eGlassy carbon electrode.

Table II. Comparison of the present NO_3^- biosensor along with the standard griess method for the measurement of NO_3^- in the beetroot juice.

No. of experiments	Nitrate conc. by griess method (μM)	Nitrate conc. by biosensor (μM)
01	593 \pm 11.8	590 \pm 11.8
02	612 \pm 12.2	610 \pm 12.2
03	601 \pm 12.0	600 \pm 12.0

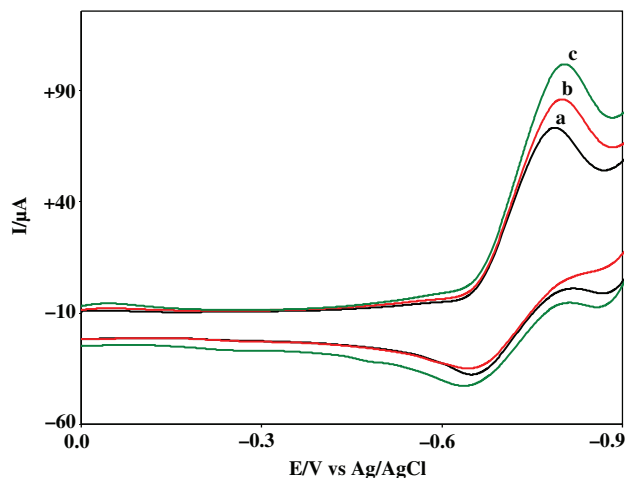


Fig. 8. Typical electrochemical response of the NaR-SAM-GNP-PPy-Pt electrode for MCF-7 cells treated with (a) control, (b) 50 ng LPS and (c) 100 ng LPS in 0.1 M PBS (pH 7.0) at scan rate: 50 mV s⁻¹ versus Ag/AgCl.

and the results obtained using both the methods were compared as shown in Table II.

3.9. Measurement of NO₃⁻ Release from LPS Treated MCF-7 Human Breast Cancer Cells

Earlier studies reported that the NO₃⁻, stable end product of NO, NO₂⁻ is generated by breast cancer cells when exposed to LPS.⁹ We have estimated here the NO₃⁻ release from LPS treated MCF-7 cells using the developed NO₃⁻ biosensor. After 24 hrs stimulation by 50 ng LPS the cathodic peak current at -0.76 V clearly increased compared to control and found that the concentration of NO₃⁻ released from the MCF-7 cells is 86.5 ± 1.73 μM (Fig. 8). The cathodic peak current of the 100 ng LPS stimulation was also investigated and found that 200.4 ± 4.0 μM of NO₃⁻ was released. Thus LPS dose dependently stimulated NO₃⁻ release from the cancer cells. The concentrations of the NO₃⁻ levels generated from the cancer cells determined were in agreement with the reference method.⁹

4. CONCLUSION

A highly sensitive and selective NO₃⁻ biosensor in which NaR was covalently linked to the SAM of cysteine on GNP in PPy matrix has been reported. The efficient combination of SAM on GNP in microporous PPy matrix enhanced the effective loading and electrocatalytic activities of NaR without their denaturation. The direct electron transfer facilitated between the electrode and the active site of the NaR provided a highly sensitive method for the determination of NO₃⁻. The fabricated NO₃⁻ biosensor also exhibited good reproducibility and long term stability. This NO₃⁻ biosensor was further applied to the NO₃⁻ determination in beetroot juice samples and human breast cancer cells.

Abbreviations

AsA	Ascorbic acid
CV	Cyclic voltammetry
GNP	Gold nanoparticles
HAuCl ₄ ·3H ₂ O	Chloroauric acid trihydrate
LPS	Lipopolysaccharide
NaR	Nitrate reductase
NO	Nitric oxide
NO ₂ ⁻	Nitrite
NO ₃ ⁻	Nitrate
PBS	Phosphate buffer solution
PPy	Polypyrrole
Pt	Platinum
SAM	Self-assembled monolayer
SEM	Scanning electron microscopy
UA	Uric acid

Acknowledgments: This work was supported by the DIPAS-DRDO, New Delhi, India (Grant No. TC/341/Task-165(CKK)/DIPAS/2010), and the Managing Board of Virudhunagar Hindu Nadar's Senthikumar Nadar College, Virudhunagar, Tamil Nadu, India. Ramanujan Fellowship to KS from DST and Senior Research Fellowship to AKK from CSIR, India are greatly acknowledged.

References and Notes

- S. R. Tannenbaum and P. Correa, *Nature* 317, 675 (1985).
- J. O. Lundberg, E. Weitzberg, and M. T. Gladwin, *Nat. Rev. Drug Discov.* 7, 156 (2008).
- A. J. Webb et al., *Hypertension* 51, 784 (2008).
- F. J. Larsen, E. Weitzberg, J. O. Lundberg, and B. Ekblom, *Acta Physiol. (Oxf)* 191, 59 (2007).
- J. O. Lundberg et al., *Nat. Chem. Biol.* 5, 865 (2009).
- A. A. Kenjale et al., *J. Appl. Physiol.* 110, 1582 (2011).
- K. J. Joshipura et al., *Ann. Intern. Med.* 134, 1106 (2001).
- F. L. Crowe et al., *Eur. Heart J.* 32, 1235 (2011).
- S. Kotamraju, C. L. Williams, and B. Kalyanaraman, *Cancer Res.* 67, 7386 (2007).
- N. Beda and A. Nedospasov, *Nitric Oxide* 13, 93 (2005).
- Y. Xuan-Feng, Z. Zhi-Qi, and Y. Hong-Tao, *Talanta* 62, 97 (2004).
- J. W. Aylotta, D. J. Richardson, and D. A. Russell, *Analyst* 122, 70 (1997).
- R. T. Masserini and K. A. Fanning, *Mar. Chem.* 68, 323 (2000).
- J. R. E. Thabano, D. Abongo, and G. M. Sawula, *J. Chromatogr. A* 1045, 153 (2004).
- S. J. R. Prabakar and S. S. Narayanan, *Electroanalysis* 21, 1481 (2009).
- S. Rajesh, U. S. E. Arivudainambi, S. Raja Singh, A. Rajendran, S. Kotamraju, and C. Karunakaran, *Sens. Lett.* 8, 1 (2010).
- S. Rajesh, A. Koteswararao, K. Bhargava, G. Ilavazhagan, S. Kotamraju, and C. Karunakaran, *Biosensors Bioelec.* 26, 689 (2010).
- P. Dharmapandian, S. Rajesh, S. Rajasingh, A. Rajendran, and C. Karunakaran, *Sens. Actuators B* 148, 17 (2010).
- L. M. Moretto, P. Ugo, M. Zanata, P. Guerriero, and C. R. Martin, *Anal. Chem.* 70, 2163 (1998).

20. M. Badea, A. Amine, G. Palleschi, D. Moscone, G. Volpe, and A. Curulli, *J. Electroanal. Chem.* 509, 66 (2001).
21. D. Kirstein, L. Kirstein, F. Scheller, H. Borchering, J. Ronner, S. Dieckmann, and P. Steinrucke, *J. Electroanal. Chem.* 474, 43 (1999).
22. S. Cosnier, C. Innocent, and Y. Jouannea, *Anal. Chem.* 66, 3198 (1994).
23. J. C. M. Gamboa, R. C. Pena, T. R. L. C. Paixao, and M. Bertotti, *Talanta* 80, 581 (2009).
24. M. T. D. Groot and M. T. M. Koper, *J. Electroanal. Chem.* 562, 81 (2004).
25. D. Quan, J. H. Shim, J. D. Kim, H. S. Park, G. S. Cha, and H. Nam, *Anal. Chem.* 77, 4467 (2005).
26. S. Reiter, K. Habermuller, and W. Schuhmann, *Sens. Actuators B* 79, 150 (2001).
27. T. Ahuja, I. Ahmad Mir, D. Kumar, and Rajesh, *Sens. Actuators B* 134, 140 (2008).
28. J. Manso, M. L. Mena, P. Y. Seden, and J. M. Pingarron, *Anal. Biochem.* 375, 345 (2008).
29. P. Raveendran, J. Fu, and S. L. Wallen, *Green Chem.* 8, 34 (2006).
30. I. Becerik, and F. Kadirgan, *Elec. Chim. Acta* 42, 283 (1997).
31. V. Tsakova, L. Sabbatinia, and P. G. Zambonin, *Mater. Chem.* 11, 1434 (2001).
32. L. Xiaofeng, C. Danming, C. Jingyu, Z. Wanjin, and W. Yen, *Mater. Lett.* 60, 2851 (2006).
33. R. Zhu, G. Li, and G. Huang, *Mater. Corros.* 60, 34 (2009).
34. S. E. Moulton, J. N. Barisci, A. Bath, R. Stella, and G. G. Wallace, *Elec. Chim. Acta* 49, 4223 (2004).
35. A. Mortari, Ph.D Thesis, Lund University (2008).
36. X. Wang, S. V. Dzyadevych, J. M. Chovelon, N. J. Renault, L. Chen, S. Xia, and J. Zhao, *Talanta* 69, 450 (2006).
37. N. F. Ferreyra and V. M. Sol, *Bioelectrochem.* 64, 61 (2004).
38. M. Sohail and S. B. Adeloju, *Sens. Actuators B* 133, 333 (2008).

Delivered by Publishing Technology to: Ecole polytechnique federale de Lausanne
IP: 128.178.39.153 On: Mon, 29 Sep 2014 11:27:15
Copyright: American Scientific Publishers